Importance of the Apical Site of the $(H_2PC_2H_4PH_2)Pd$ Complex on the Elementary Reactions. A Density Functional Study

Toshiaki Matsubara*,†,‡ and Kazuyuki Hirao‡

Institute for Fundamental Chemistry, 34-4 Takano-Nishihiraki-cho, Sakyo-ku, Kyoto 606-8103, Japan, and Department of Material Chemistry, Graduate School of Engineering, Kyoto University, Sakyo-ku, Kyoto 606-8501, Japan

Received February 14, 2002

The importance of the apical site of the palladium complex on the elementary reactions is theoretically examined with a density functional method (B3LYP) using the model complex $(H_2PC_2H_4PH_2)Pd$. It is well-known by many theoretical analyses that the oxidative addition and reductive elimination of the chemical bonds, such as H−H and C−H, on the phosphine-coordinated palladium complex, $(PH_3)_2Pd$, take place in the equatorial plane by the charge transfers between the d and sp orbitals of the Pd enhanced by the equatorial phosphine ligands and the bonding and antibonding orbitals of the chemical bonds. Therefore, the role of the fifth site at the apical position has not been known so far. In the present study, we successfully suggested the important role of the apical site to significantly stabilize the potential surface of the reaction and lower the energy barrier, on the oxidative addition of the C−X (X = Sn, Ge, Si, C) bonds of heteroles to the Pd of $(H_2PC_2H_4PH_2)Pd$ and the insertion of XH_2 into the Pd−C bond of $(H_2PC_2H_4PH_2)Pd(\eta^2\text{-}HC{\equiv}CH)$. In the insertion reaction, the effect of the apical site increases in the order Sn < Ge < Si. On the other hand, in the oxidative addition of the C−X bond of heteroles $C_4H_4XH_2$, this order is reversed, i.e., Sn > Ge > Si > C, which indicates that the importance of the apical site increases in the case for the strongly polarized C−X bond. However, the apical site was invalid for the oxidative addition of the C−X bond of CH_3XH_3, which has no π orbital on the C−X carbon promoting the charge transfer on the apical site. The possibility of the intramolecular rearrangement of the $(H_2PC_2H_4PH_2)Pd(H)(XH_3)$ complex which switches the position of the hydrido and XH_3 ligands utilizing the apical site was also suggested.

1. Introduction

We recently reported a density functional study[1] for the [2+2+1] cycloaddition reaction of two ethynes and one stannylene to form stannole. The stannoles (C_4H_4)-SnR'_2 are produced from SnR'_2 ($R' = CH(SiMe_3)_2$ or $R'_2 = \{C(SiMe_3)_2CH_2\}_2$) and ethyne at a low temperature by the phosphine-coordinated palladium catalysts $(PR_3)_2Pd$ or $(R_2PC_2H_4PR_2)Pd$ (R = Me, i-Pr, t-Bu) in experiment.[2] Possible reaction paths for the entire catalytic cycle were proposed by Pörschke et al.[2b] on the basis of their experimental analysis, as depicted in Figure 1.

In the first process—the formation of the 1,2-metallastannete intermediate **4′** from the starting complex **1′**—two pathways, which are denoted by paths a and b, are considered, because the reactant **1′** can give two adducts **2′** and **5′** by the coordination of ethyne and SnR_2, respectively. In path a, the η^2-ethyne-π-complex **2′** formed from **1′** with ethyne undergoes the insertion

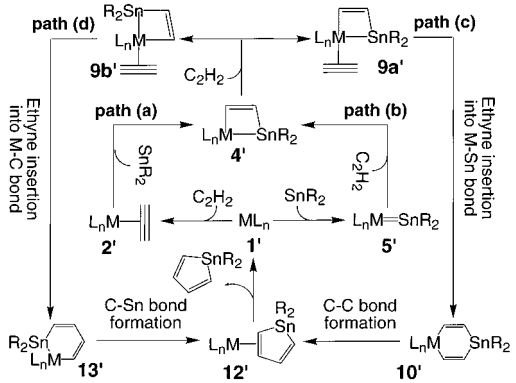

Figure 1. A possible catalytic cycle for the stannole formation.

of the stannylene SnR'_2, which leads **2′** to the 1,2-metallastannete intermediate **4′**. On the other hand, in path b, the stannylene first coordinates to the Pd of **1′** to form the stannylene complex **5′**, which is followed by the addition of the ethyne to the Pd═Sn bond of **5′**. We have already theoretically examined in detail path b.[1,3] The subsequent process starting from **4′** also has

† Institute for Fundamental Chemistry.
‡ Kyoto University.

(1) Sahnoun, R.; Matsubara, T.; Yamabe, T. *Organometallics* **2000**, *19*, 5661.

(2) (a) Krause, J.; Pluta, C.; Pörschke, K.-R.; Goddard, R. *J. Chem. Soc., Chem. Commun.* **1993**, 1254. (b) Krause, J.; Haack, K.-J.; Pörschke, K.-R.; Gabor, B.; Goddard, R.; Pluta, C.; Seevogel, K. *J. Am. Chem. Soc.* **1996**, *118*, 804.

(3) (a) Matsubara, T. *Organometallics* **2001**, *20*, 1462. (b) Matsubara, T.; Hirao, K. *J. Am. Chem. Soc.* **2002**, *124*, 679. (c) Matsubara, T.; Hirao, K. *Organometallics* **2002**, *21*, 1697.

10.1021/om020119b CCC: $22.00
Publication on Web 05/31/2002

alternative paths c and d after the dissociation of a PH_3 ligand, which depends on the position of the incoming ethyne in the intermediate **9′**, i.e., cis or trans to Sn. In path c, the coordinated ethyne is inserted into the M−Sn bond in **9a′**, leading to **10′**, and then C−C coupling takes place to produce the product, stannole. In another path, d, the coordinated ethyne is inserted into the M−C bond in **9b′**, leading to **13′**, and then C−Sn coupling takes place.

According to our previous computational study[1] for the full catalytic cycle proposed by Pörschke et al., where the model complex $(PH_3)_2Pd$ as a precursor catalyst **1′** and stannylene SnH_2 were used, the catalytic reaction selects the energetically favorable path b in the first process and path c in the second process of the catalytic cycle. However, it is very interesting that our calculations suggested the importance of the apical site of the palladium complex in paths a and d. In path a, the insertion of stannylene to form the metallacycle intermediate **4′** from the η^2-ethyne-π-complex **2′** passes through an intermediate in which stannylene coordinates to the apical site. On the other hand, in the transition state of the C−Sn bond formation in path d, the C−Sn axis is perpendicular to the P−Pd−P plane and the Sn atom is placed at the apical position. This means that in the reverse reaction the C−Sn bond of stannole approaches the Pd atom not parallel but perpendicular to the P−Pd−P plane to break the C−Sn bond. In sharp contrast to this transition state structure, the transition state in the C−C bond formation in path c has the C−C axis parallel to the P−Pd−P plane, as well-known for the σ bond activation of H−H and C−H[4,5] on the phosphine-coordinated palladium or platinum complex $(PH_3)_2M$ (M = Pd, Pt). The fact that the H−H and C−H bond axes are parallel to the P−Pd−P plane in the transition states is quite reasonable, because the electron back-donation, which plays a key role in the bond breaking, occurs from the dπ orbital enhanced in the P−Pd−P plane to the H−H or C−H σ* orbital as presented below:

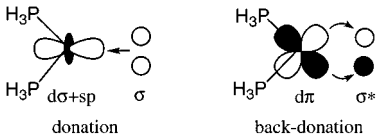

Therefore, now the following questions arise; Why is the C−Sn axis perpendicular to the P−Pd−P plane in the transition state? Where does the difference between Sn and C come from? What about the other atoms, Ge and Si, in the same group?

In the present study, to find an answer to these questions, we further theoretically investigated the elementary steps in detail with the density functional method (B3LYP) apart from the catalytic cycle. We especially give an insight from the viewpoint of the role of the apical site of the palladium complex, although the importance of the apical site has been little discussed so far. As the palladium complex, we selected the model complex having a chelate phosphine ligand, $(H_2PC_2H_4PH_2)Pd$. In addition to the insertion of XH_2 (X = Sn, Ge, Si, C) into the Pd−C bond of $(H_2PC_2H_4PH_2)Pd(\eta^2\text{-}HC{\equiv}CH)$ and the oxidative addition of the C−X bonds of heterocyclopentadienes (heteroles) $C_4H_4XH_2$ to $(H_2PC_2H_4PH_2)Pd$, the basic organometallic reaction, the oxidative addition of the C−X bonds of CH_3XH_3 to $(H_2PC_2H_4PH_2)Pd$, was examined. The possibility of the intramolecular rearrangement of the hydrido complex $(H_2PC_2H_4PH_2)Pd(H)(XH_3)$, which mutually switches the positions of the hydrido and the XH_3 ligands by support of the apical site without the dissociation of XH_4, was also examined. Following the explanation of computational procedures in section 2, the insertion reaction is first discussed in section 3.1, and then the oxidative addition in the subsequent sections, 3.2 and 3.3. The intramolecular rearrangement is discussed in section 3.4. Conclusions are summarized in the last section.

2. Computational Procedures

All calculations were performed using the Gaussian98 program.[6] The calculations of energetics as well as geometry optimizations were carried out at the B3LYP level of theory, which consists of a hybrid Becke + Hartree−Fock exchange and a Lee−Yang−Parr correlation functional with nonlocal corrections.[7] The basis set used, hereinafter referred to as BSI, is the 6-31G** level for the H, C, and Si atoms of ethyne, XH_2, XH_4, CH_3XH_3, and heteroles, $C_4H_4XH_2$ (X = Sn, Ge, Si, C), and the 6-31G level for the C and H atoms and the 6-31G* level for the P atom of the spectator ligand $H_2PC_2H_4PH_2$. For Pd, the triple-ζ (5s,6p,4d,1f)/[3s,3p,3d,1f] augmented by an additional single set of f orbitals with the exponent of 1.472[8] and the effective core potential (ECP) determined by Hay−Wadt[9] to replace the core electrons except for the 18 electrons in the valence shell, and for Sn and Ge, the (3s,3p)/[2s,2p] basis functions with a polarization function, i.e., 5d with the exponent of 0.183[10] for Sn and 4d with the exponent of 0.246[10] for Ge, and the Hay−Wadt ECP[11] to replace the core electrons except for the four valence electrons were used.

All equilibrium structures and transition states were optimized without any symmetry restrictions and identified by the number of imaginary frequencies calculated from the analytical Hessian matrix. The reaction coordinates were followed from the transition state to the reactant and the product by the intrinsic reaction coordinate (IRC) technique.[12] The important structures on the reaction coordinates are arbitrarily

(4) (a) Low, J. J.; Goddard, W. A., III. *J. Am. Chem. Soc.* **1984**, *106*, 6928. (b) Obara, S.; Kitaura, K.; Morokuma, K. *J. Am. Chem. Soc.* **1984**, *106*, 7482.

(5) (a) Low, J. J.; Goddard, W. A., III. *J. Am. Chem. Soc.* **1984**, *106*, 8321. (b) Low, J. J.; Goddard, W. A., III. *Organometallics* **1986**, *5*, 609. (c) Low, J. J.; Goddard, W. A., III. *J. Am. Chem. Soc.* **1986**, *108*, 6115.

(6) Frisch, M. J.; Trucks, G. W.; Schlegel, H. B.; Scuseria, G. E.; Robb, M. A.; Cheeseman, J. R.; Zakrzewski, V. G.; Montgomery, J. A., Jr.; Stratmann, R. E.; Burant, J. C.; Dapprich, S.; Millam, J. M.; Daniels, A. D.; Kudin, K. N.; Strain, M. C.; Farkas, O.; Tomasi, J.; Barone, V.; Cossi, M.; Cammi, R.; Mennucci, B.; Pomelli, C.; Adamo, C.; Clifford, S.; Ochterski, J.; Petersson, G. A.; Ayala, P. Y.; Cui, Q.; Morokuma, K.; Malick, D. K.; Rabuck, A. D.; Raghavachari, K.; Foresman, J. B.; Cioslowski, J.; Ortiz, J. V.; Stefanov, B. B.; Liu, G.; Liashenko, A.; Piskorz, P.; Komaromi, I.; Gomperts, R.; Martin, R. L.; Fox, D. J.; Keith, T.; Al-Laham, M. A.; Peng, C. Y.; Nanayakkara, A.; Gonzalez, C.; Challacombe, M.; Gill, P. M. W.; Johnson, B. G.; Chen, W.; Wong, M. W.; Andres, J. L.; Head-Gordon, M.; Replogle, E. S.; Pople, J. A. *Gaussian 98*; Gaussian, Inc.: Pittsburgh, PA, 1998.

(7) (a) Lee, C.; Yang, W.; Parr, R. G. *Phys. Rev. B* **1988**, *37*, 785. (b) Becke, D. *J. Chem. Phys.* **1993**, *98*, 5648.

(8) Ehlers, A. W.; Böhme, M.; Dapprich, S.; Gobbi, A.; Höllwarth, A.; Jonas, V.; Köhler, K. F.; Stegmann, R.; Veldkamp, A.; Frenking, G. *Chem. Phys. Lett.* **1993**, *208*, 111.

(9) Hay, P. J.; Wadt, W. R. *J. Chem. Phys.* **1985**, *82*, 299.

(10) Huzinaga, S. *Physical Sciences Data 16, Gaussian Basis Sets for Molecular Calculations*; Elsevier: Amsterdam, 1984.

(11) Wadt, W. R.; Hay, P. J. *J. Chem. Phys.* **1985**, *82*, 284.

(12) Fukui, K.; Kato, S.; Fujimoto, H. *J. Am. Chem. Soc.* **1975**, *97*, 1.

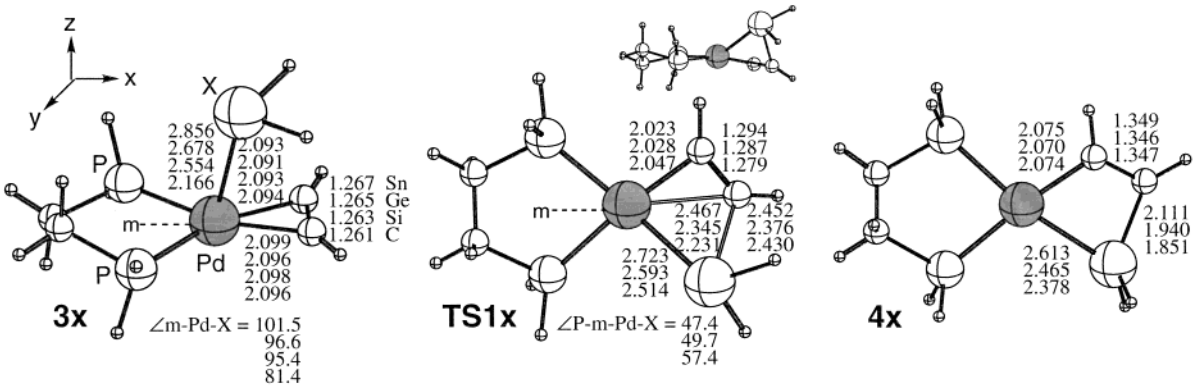

Figure 2. B3LYP/BSI-optimized structures (in Å and deg) of the intermediates **3**, transition states **TS1**, and the products **4** for the insertion of XH_2 (X = Sn, Ge, Si, C) into the Pd−C bond of the $(H_2PC_2H_4PH_2)Pd(\eta^2\text{-HC}{\equiv}\text{CH})$ complex **2**. Sideview is presented for **TS1**. m is the midpoint between two P atoms.

selected to know the reaction processes and displayed together with the optimized structures in Figures 3 and 7. NBO analysis[13] was performed to obtain the atomic orbital (AO) population and the charge. For the oxidative addition and the intramolecular rearrangement of the hydrido complex, the energies relative to the free molecules, XH_4, CH_3XH_3, and heteroles $C_4H_4XH_2$, and the $(H_2PC_2H_4PH_2)Pd$ fragment are shown. In the case of the insertion reaction, the energies relative to the free XH_2 and the $(H_2PC_2H_4PH_2)Pd(\eta^2\text{-HC}{\equiv}\text{CH})$ complex are presented. The labels for the structures, **sn**, **ge**, **si**, and **c**, are used for the atom X, i.e., Sn, Ge, Si, and C, of XH_2, XH_4, CH_3XH_3, and heteroles $C_4H_4XH_2$, respectively.

3. Results and Discussion

3.1. Insertion of XH_2 (X = Sn, Ge, Si, C) into the Pd−C Bond of the $(H_2PC_2H_4PH_2)Pd(\eta^2\text{-HC}{\equiv}\text{CH})$ Complex. The η^2-ethyne-π-complex $(H_2PC_2H_4PH_2)Pd(\eta^2\text{-HC}{\equiv}\text{CH})$ **2** has a square planar structure with C_2 symmetry. The ethyne coordinates to the Pd parallel to the P−Pd−P plane by electron donation from the ethyne π orbital to the hybridized dσ+sp orbital of the Pd and back-donation from the dπ orbital of the Pd enhanced by the bend of the P−Pd−P axsis[14] to the π^* orbital of ethyne, which is well-known as a Dewar−Chatt−Duncanson model.[15] Surprisingly, the SnH_2 molecule coordinates to the apical site of complex **2** to form **3sn,** as displayed in Figure 2, although the coordination to the apical site of the palladium π-complex **2** has not been known so far. Even if the positions were artificially switched to each other between the ethyne at the equatorial and the stannylene at the apical position, **3sn** was finally obtained by the geometry optimization.

In **3sn**, SnH_2 occupies the apical position, interacting with the Pd by two kinds of charge transfer. As shown in Table 1, not only the donation of the lone pair electron of Sn to the Pd but also the electron back-donation from the Pd d orbital to the unoccupied p orbital of the Sn occurs. By these interactions between the Sn and Pd atoms, the population of both the lone pair electron of the Sn and the d_{xz} orbital of the Pd is reduced. We could not extract successfully the pure population for the unoccupied p orbital of the Sn. The total charge of SnH_2 increased to $-0.193e$ by the coordination, suggesting that the electron back-donation from the Pd d_{xz} orbital to the unoccupied p orbital of the Sn is dominant in the interaction (see illustration I presented below). It should

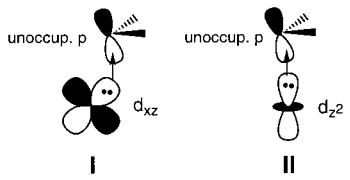

be noted here that the other molecule only with the lone pair electron, for example H_2O and NH_3, did not coordinate to the apical site of **2**. The coordinated SnH_2 at the apical position slightly inclines toward the ethyne ligand at the equatorial position, deforming the square-pyramidal structure, as shown by the angle ∠Sn−Pd−m, which is larger than 90°, due to the contribution of the lone pair electron of the Sn in the coordination.

Even though the Sn atom was replaced by the other atoms, Ge, Si, C, in the same group, the similar structures **3** were obtained. However, the angle ∠X−Pd−m decreased in the order Sn > Ge > Si > C, and the stability of the complexes **3** relative to **2** increased in the order C (30.2 kcal/mol) > Si (20.9 kcal/mol) > Ge (18.1 kcal/mol) > Sn (17.0 kcal/mol). As shown by the negative charge of XH_2 with the sequence C > Si > Ge > Sn, the electron back-donation from the Pd to the unoccupied p orbital of the atom X increases in the same order. As a result, the electron back-donation from the Pd to the X p orbital rather than the donation of the lone pair electron of the X to the Pd becomes significant, which is reflected in the angle ∠X−Pd−m. Therefore, the electron back-donation occurs from both d_{xz} and d_{z^2} orbitals for X = Ge and from only the d_{z^2} orbital in the case of X = Si and C, as illustrated above. The population of the 5s orbital of the Pd is also markedly reduced by the electron back-donation for X = C, because the unoccupied p(p_z) orbital of CH_2 is lying lower in energy compared with those of the other XH_2, as shown in Table 1. Both the C−C bond of ethyne and the Pd−C(ethyne) bonds at the equatorial position are little affected by the coordination of XH_2.

The coordinated stannylene at the apical position moves into the equatorial plane without dissociation,

(13) Glendening, E. D.; Reed, A. E.; Carpenter, J. E.; Weinhold, F. *NBO Version 3.1*.
(14) Saillard, J.-Y.; Hoffmann, R. *J. Am. Chem. Soc.* **1984**, *106*, 2006.
(15) (a) Dewar, M. J. S. *Bull. Soc. Chim. Fr.* **1951**, C71. (b) Chatt, J.; Duncanson, L. A. *J. Chem. Soc.* **1953**, 2939.

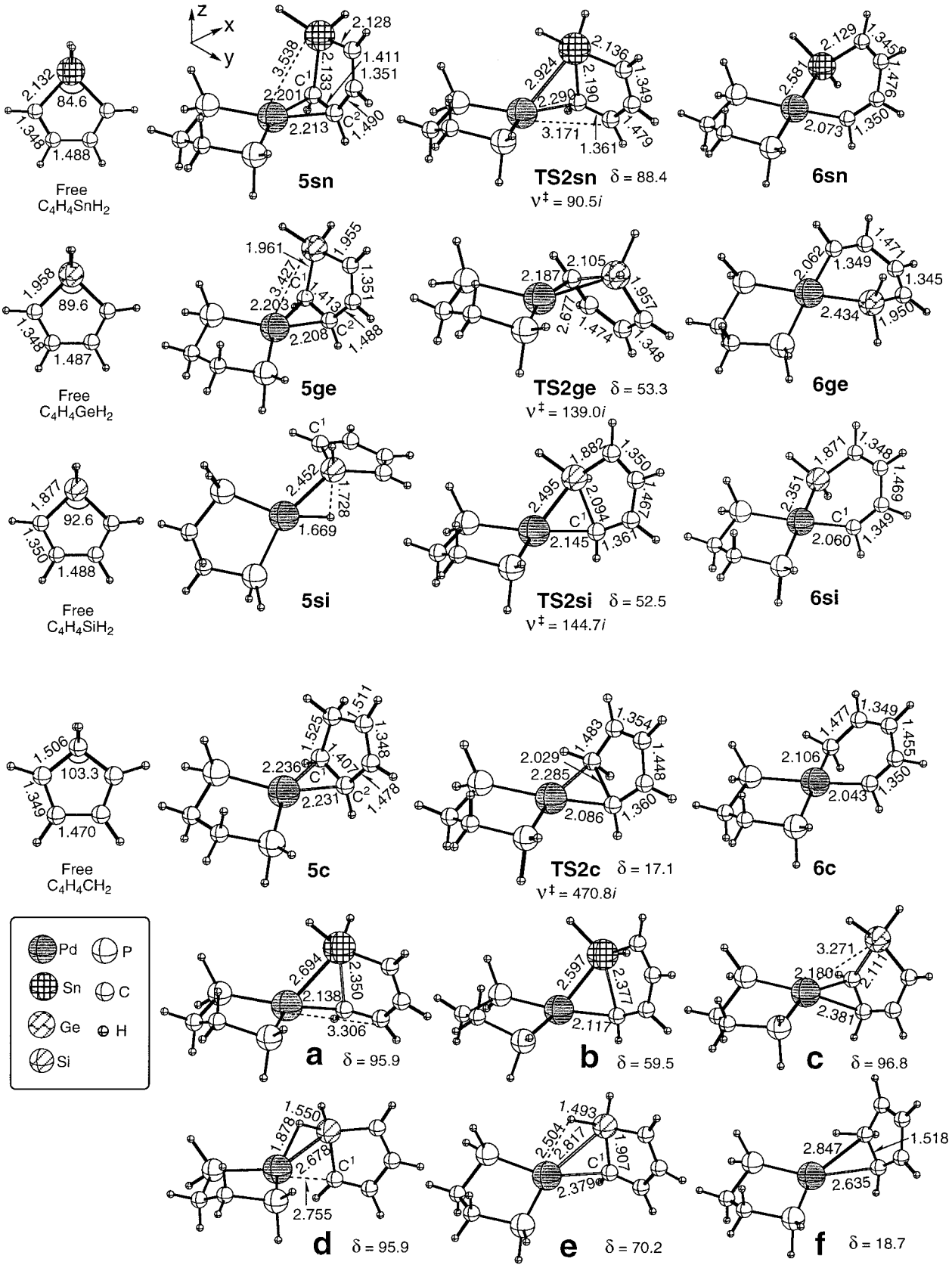

Figure 3. B3LYP/BSI-optimized structures (in Å and deg) of the intermediates **5**, transition states **TS2**, and the products **6** for the oxidative addition of the C−X bonds of heteroles $C_4H_4XH_2$ (X = Sn, Ge, Si, C) to the $(H_2PC_2H_4PH_2)Pd$ complex **1**, together with those of the free heteroles, and the snapshots of the structures **a**−**f** at points a−f (see Figure 5) on the potential energy surfaces of the reaction. The imaginary frequencies (cm^{-1}) are shown for the transition states **TS2**. δ is the dihedral angles ∠P−m−Pd−H for **d** and ∠P−m−Pd−X for the others (m is the midpoint between two P atoms).

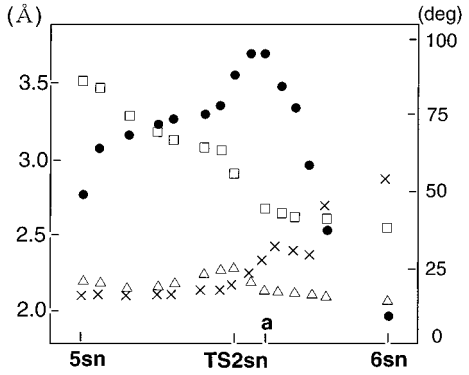

Figure 4. Changes in the geometric parameters during the oxidative addition of the C−Sn bond of stannole $C_4H_4SnH_2$ to the $(H_2PC_2H_4PH_2)Pd$ complex **1**: (●) ∠P−m−Pd−Sn; (□) *d*(Pd−Sn); (△) *d*(Pd−C[1]); (×) *d*(C−Sn). m is the midpoint between two P atoms.

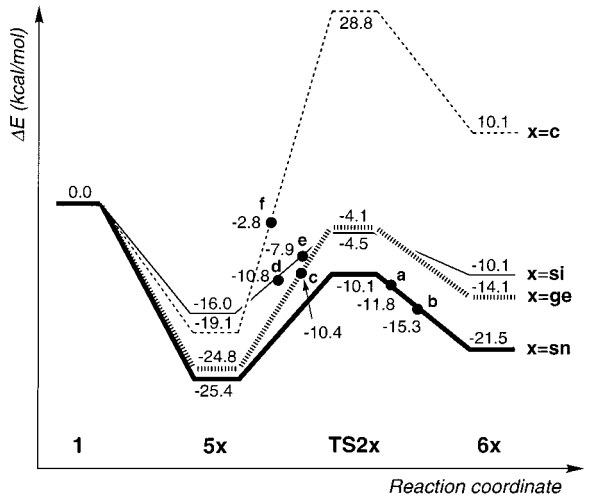

Figure 5. B3LYP/BSI potential energy surfaces (in kcal/mol) of the oxidative addition of the C−X bonds of heteroles $C_4H_4XH_2$ (X = Sn, Ge, Si, C) to the $(H_2PC_2H_4PH_2)Pd$ complex **1**. The boldface, boldface-dotted, normal, and dotted lines are for X = Sn, Ge, Si, C, respectively. The energies relative to **1** are presented.

reducing the dihedral angle ∠P−m−Pd−X, and is inserted into the Pd−C(ethyne) bond to form the complex **4**, which has a square planar structure with C_s symmetry, as presented in Figure 2. In the transition state **TS1**, the unoccupied p orbital of the atom X bridges over the Pd and one of the ethyne C atoms through the electron back-donation from both Pd d_{xz} and ethyne π orbitals. This interaction of the X with the Pd by the electron back-donation from the Pd d_{xz} to the unoccupied p orbital of the atom X during the reaction significantly stabilizes the potential energy surface, so that a small energy barrier of less than 10 kcal/mol is required (see Table 2).[16] The potential energy surface was more stabilized in the order Si > Ge > Sn, and the energy barrier was reduced in the reversed order, because the electron back-donation becomes stronger

(16) In the other insertions, energy barriers that are much larger than 10 kcal/mol have been reported. For example, see: (a) Sakaiki, S.; Kitaura, K.; Morokuma, K.; Ohkubo, K. *J. Am. Chem. Soc.* **1983**, *105*, 2280. (b) Koga, N.; Morokuma, K. *J. Am. Chem. Soc.* **1985**, *107*, 7230. (c) Koga, N.; Morokuma, K. *J. Am. Chem. Soc.* **1986**, *108*, 6136.

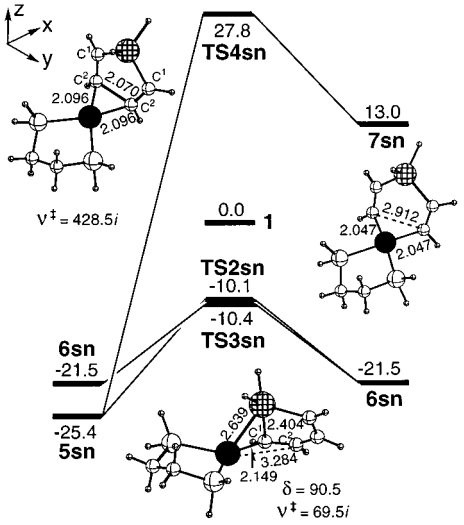

Figure 6. B3LYP/BSI potential energy surfaces (in kcal/mol) of the oxidative addition of the C−Sn (**5sn**→**TS2sn**→**6sn**) and the C^2−C^2 (**5sn**→**TS4sn**→**7sn**) bonds of stannole to the $(H_2PC_2H_4PH_2)Pd$ complex **1**, and the intramolecular rearrangement of **6sn** through the transition state **TS3sn** (**6sn**→**TS3sn**→**6sn**), together with the optimized structures (in Å and deg) of the transition states **TS3sn** and **TS4sn**, and the product **7sn** at the B3LYP/BSI level. The imaginary frequencies (cm^{-1}) are shown for the transition states **TS3sn** and **TS4sn**. δ is the dihedral angle ∠P−m−Pd−Sn (m is the midpoint between two P atoms). The energies relative to **1** are presented.

with the order Si > Ge > Sn, according to the energy level of the unoccupied p orbital of XH_2 (see Table 1). We did not follow the reaction coordinate throughout for X = C, because the mechanism was different from the others, which probably originates from the electronic character of methylene CH_2.

3.2. Oxidative Addition of the C−X Bonds of Heteroles $C_4H_4XH_2$ (X = Sn, Ge, Si, C) to the $(H_2PC_2H_4PH_2)Pd$ Complex. In this section, the oxidative addition of the C−X bonds of heteroles $C_4H_4XH_2$ (X = Sn, Ge, Si, C) to the $(H_2PC_2H_4PH_2)Pd$ complex is discussed. In the case of X = Sn, the incoming stannole coordinates to the Pd atom of the $(H_2PC_2H_4PH_2)Pd$ complex through the η^2-C=C π interaction in the P−Pd−P plane to form the intermediate **5sn**, as presented in Figure 3. One of the coordinated carbons dissociates from the Pd atom, and the C−Sn axis approaches the Pd atom in the transition state **TS2sn**. Here, it is very surprising that the C−Sn axis is nearly perpendicular to the P−Pd−P plane, as shown by the dihedral angle δ of 88.4°. The dihedral angle δ is reduced by the rotation of the C−Sn axis and becomes zero in the product **6sn**. These structural features of **TS2sn** are quite unique, because the bond axis to be broken is usually parallel to the P−Pd−P plane in the transition state, as reported for the H−H and C−H bond breaking in the $(PH_3)_2M$ (M = Pt, Pd) complexes.[4,5] In fact, the C−C axis was almost parallel to the P−M−P plane in the transition state of the C^2−C^2 bond breaking of stannole, as mentioned later (see Figure 6). It should be noted here that the C atom occupies the equatorial position, while the Sn atom the apical position in **TS2sn**, which is quite important to understand the role of the apical site.

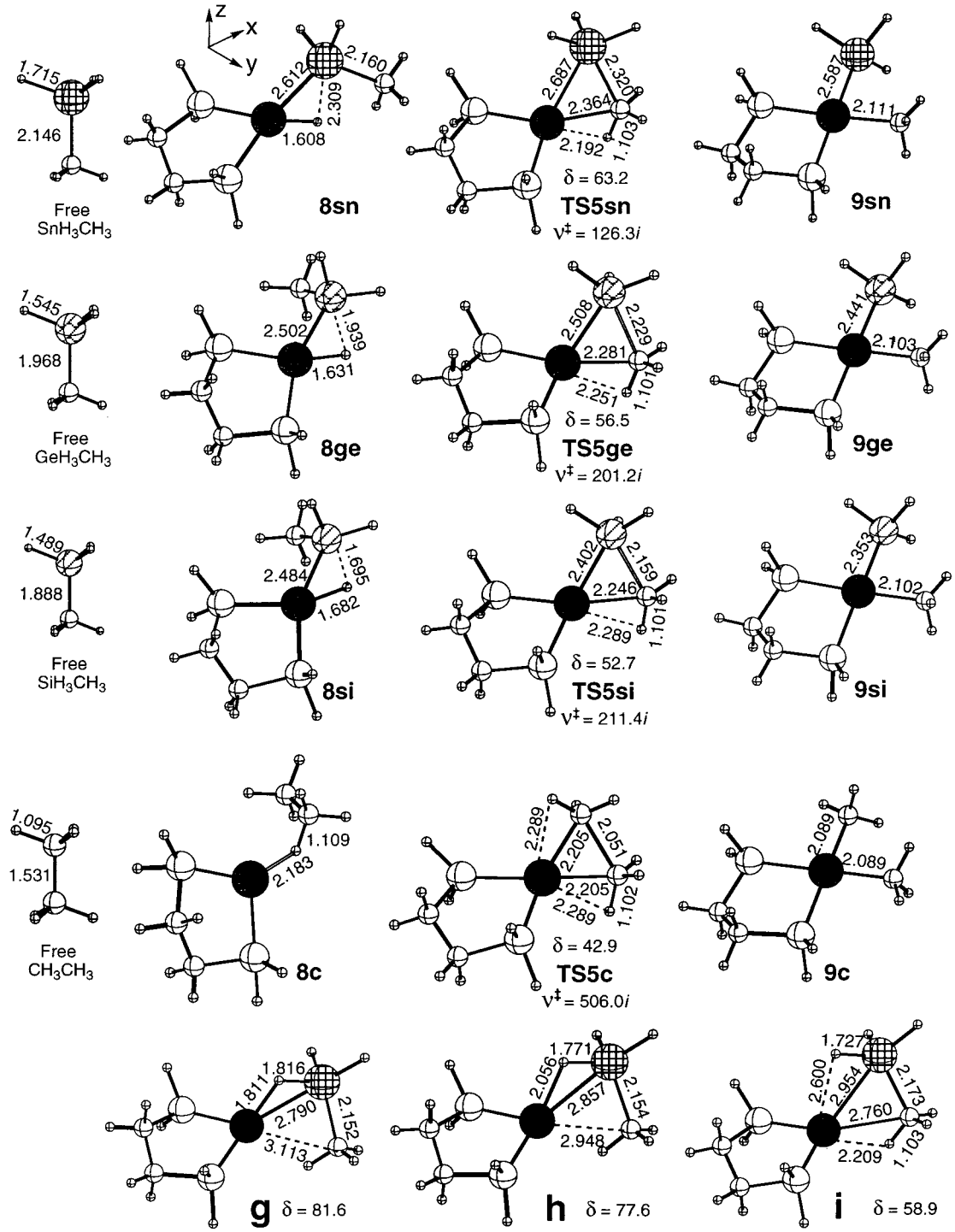

Figure 7. B3LYP/BSI-optimized structures (in Å and deg) of the intermediates **8**, transition states **TS5**, and the products **9** for the oxidative addition of the C−X bonds of CH_3XH_3 (X = Sn, Ge, Si, C) to the $(H_2PC_2H_4PH_2)Pd$ complex **1**, together with those of the free CH_3XH_3, and the snapshots of the structures **g**−**i** at points g−i (see Figure 8) on the potential energy surfaces of the reaction. The imaginary frequencies (cm^{-1}) are shown for the transition states **TS5**. δ is the dihedral angles ∠P−m−Pd−H for **g** and **h**, and ∠P−m−Pd−X for the others (m is the midpoint between two P atoms).

To know how the C−Sn bond is broken on the $(H_2PC_2H_4PH_2)Pd$ fragment, we followed the structural change throughout the reaction. The change in the selected geometrical parameters during the reaction from **5sn** to **6sn** through the transition state **TS2sn** is presented in Figure 4. The dihedral angle ∠P−m−Pd−Sn shows a maximum around point a just after the transition state **TS2sn**, and both Pd−Sn and Pd−C[1] distances are significantly shortened and become almost the same as those in the product **6sn** before reaching point a. On the other hand, the C−Sn bond is only 10% stretched at point a. The C−Sn distance is gradually lengthened after passing through point a with a decrease in the dihedral angle ∠P−m−Pd−Sn. When the dihedral angle ∠P−m−Pd−Sn becomes less than 60°, the C−Sn distance is quickly elongated.

Table 1. Atomic Orbital (AO) Population and Charge for the $(H_2PC_2H_4PH_2)Pd(XH_2)(\eta^2$-HC≡CH) (X = Sn, Ge, Si, C) 3x (x = sn, ge, si, c) and $(H_2PC_2H_4PH_2)Pd(\eta^2$-HC≡CH) 2 Complexes and Molecular Orbital (MO) Energy (in hartree) of the Free XH_2

	4d				X	charge	MO energy of the free XH_2	
	xz	z^2	5s	$5p_z$	lone pair[a]	XH_2	X (lone pair)	X (p_z)
2	1.928	1.954	0.410	0.000				
3sn	1.853	1.944	0.402	0.002	1.674 (−0.099)	−0.193	−0.465	−0.114
3ge	1.867	1.889	0.394	0.001	1.642 (−0.107)	−0.231	−0.508	−0.116
3si	1.933	1.862	0.382	0.002	1.610 (−0.110)	−0.262	−0.509	−0.119
3c	1.969	1.662	0.356	0.002	1.529 (−0.116)	−0.378	−0.667	−0.122

[a] The numbers in parentheses are the differences from those of the free XH_2.

Table 2. Calculated Energy Profiles (in kcal/mol)[a] for the Insertion of XH_2 (X = Sn, Ge, Si) into the Pd−C Bond of the $(H_2PC_2H_4PH_2)Pd(\eta^2$-HC≡CH) Complex 2 (3→TS1→4) and the Energy Differences between the Intermediates 3 and the Transition States TS1

	3x	**TS1x**	**4x**	ΔE(**3x→TS1x**)
x = sn	−17.0	−8.5	−31.2	8.5
ge	−18.1	−13.9	−45.2	4.2
si	−20.9	−19.0	−63.2	1.9

[a] Energies relative to **2** are presented.

In contrast, in the case of Ge, the Pd−Ge distance, which is more than 3 Å in the π-complex **5ge**, is maintained and the Ge atom never comes closer to the Pd atom during the rotation of the Ge−Pd−C plane. Even at point c on the reaction coordinate where δ is 96.8°, the Pd−Ge distance (3.271 Å) remains long. The Pd−Ge distance is not shortened until the Ge atom passes through the apical position by the rotation of the Ge−Pd−C^1 plane. In the case of Si, the intermediate **5si** is not the η^2-C=C π-complex but the hydrido complex. The hydrido ligand at the equatorial position bridges over the Pd−Si bond in **5si**, as shown by the short Si−H distance of 1.728 Å, because the Si atom is electron deficient. On the way from the transition state **TS2si** to the intermediate **5si**, the H−Pd−Si plane as well as the Si−Pd−C^1 plane becomes perpendicular to the P−Pd−P plane by its rotation, avoiding the electronic repulsion between the occupied d_{xy} orbital and the C^1-H σ orbital, as shown by the serial snapshots of the structure **TS2si→e→d**. Both Pd−Si and Pd−H bondings are fairly strengthened in the structure **d**, and the Si−H bond is easily activated without the energy barrier to form **5si**.[17] In the case of X = C, the CH_2 carbon in the π-complex **5c** immediately shifts to the P−Pd−P plane after the dissociation of both C^1 and C^2 atoms. The C(X)−Pd−C^1 plane is nearly parallel to the P−Pd−P plane in the transition state **TS2c**.

The stability of the heterole-π-complexes **5** showed the sequence Sn (25.4 kcal/mol) > Ge (24.8 kcal/mol) > C (19.1 kcal/mol), as presented in Figure 5. The electronic effect of the atom X obviously affects the stability and the geometry of the heterole-π-complex **5**. The Pd−C^2 bond is longer than the Pd−C^1 bond for X = Sn and Ge, indicating that the bonding is stronger for Pd−C^1 than for Pd−C^2. The difference between the Pd−C^1 and Pd−C^2 distances decreases in the order Sn > Ge, and Pd−C^1 becomes longer than Pd−C^2 for X = C. These trends are ascribed to the polarization of the C−X bond of heteroles. As presented in Table 3, in the case of Sn, the Sn−C^1 and Sn−H^1 bonds of stannole are extremely polarized and the Sn atom is electron deficient. The Sn atom has a large positive charge of 1.419*e*, whereas the C^1 and H^1 atoms have a negative charge of −0.667*e* and −0.273*e*, respectively. The negative charge of C^1 is about 2.7 times larger than that of C^2 by the electron flow from the Sn. Thus, the electron is considerably accumulated at C^1 to strongly donate the electron to the Pd. However, the difference in the charge between the C^1 and C^2 atoms decreases in the order Sn > Ge, and the negative charge at C^1 becomes smaller than that at C^2 in the case of X = C, since the C(X) attached to C^1 is negatively charged. The sequence in the energy level (in hartree) of the electron acceptor C=C π* of heteroles $C_4H_4XH_2$, C(0.1126) > Sn(0.0459) ≅ Ge(0.0449), is also reflected in the stability sequence of the heterole-π-complex **5**.

Since the electron in the Sn−C^1 is extremely localized at the C^1 for X = Sn, the electron donation from the electron-rich C^1 to the $d_{x^2-y^2}$+sp hybridized orbital of the Pd and the back-donation from the Pd d_{xz} orbital to the electron-deficient Sn occur as illustrated below:

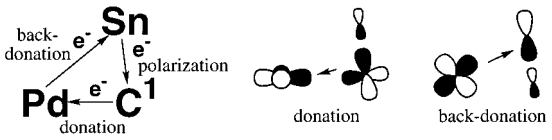

The interaction of the Sn with the Pd at the apical site originates from this charge transfer from the Pd d_{xz} orbital to the electron-deficient Sn induced by the strong polarization of the Sn−C^1 bond. The π orbital at the C^1 directed to the Pd atom would be important for the electron donation from the negatively charged C^1 to the Pd, because this charge transfer was not observed in the C−Sn bond breaking of CH_3SnH_3 (see section 3.3). The easiness of these charge transfers is also suggested by the fact that the energy level of the σ and σ* orbitals of the C−Sn bond is high and low, respectively, compared with that of those orbitals of the other C−X (X = Ge, Si, C) bonds.[18]

The contribution of the Pd d orbitals to the charge transfer interaction is sensitively reflected in their orbital population. As shown in Table 4, the population of the Pd d_{xz} orbital is reduced when the Sn−Pd−C^1 plane becomes perpendicular to the P−Pd−P plane and the Sn atom is placed at the apical position. It showed a minimum at point a on the reaction coordinate where

(17) It is well-known by the detailed theoretical analysis that the Si−H bond activation is very facile. For example, see: (a) Koga, N.; Morokuma, K. *J. Am. Chem. Soc.* **1993**, *115*, 6883. (b) Musaev, D. G.; Morokuma, K. *J. Am. Chem. Soc.* **1995**, *117*, 799.

(18) The sequence in the energy level (in hartree) of the σ and σ* orbitals of the heterole C−X (X = Sn, Ge, Si, C) bonds was as follows: σ: Sn(−0.3984) > Ge(−0.4330) > Si(−0.4880) > C(−0.5926); σ*: C(0.4355) > Ge(0.2527) ≥ Si(0.2404) > Sn(0.1580).

Table 3. NBO Analysis of the Free XH_4, CH_3XH_3, and Heteroles $C_4H_4XH_2$ (X = Sn, Ge, Si, C)

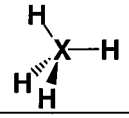

	X-H bond	Atomic Charge	
X	X%	X	H
Sn	37.2	1.011	-0.253
Ge	40.9	0.723	-0.181
Si	42.0	0.632	-0.158
C	61.6	-0.927	0.232

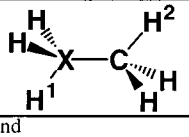

	X-C bond	X-H^1 bond	Atomic Charge		
X	X%	X%	X	C	H^1
Sn	28.1	35.9	1.253	-1.190	-0.276
Ge	29.9	39.7	1.002	-1.160	-0.204
Si	29.8	40.9	0.928	-1.166	-0.180
C	50.0	61.5	-0.685	-0.685	0.228

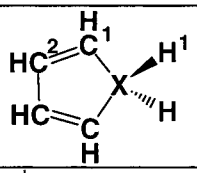

	X-C^1 bond	X-H^1 bond	Atomic Charge			
X	X%	X%	X	C^1	C^2	H^1
Sn	27.7	35.8	1.419	-0.667	-0.249	-0.273
Ge	29.6	39.7	1.203	-0.648	-0.239	-0.198
Si	29.7	41.0	1.146	-0.656	-0.229	-0.173
C	51.4	63.1	-0.530	-0.215	-0.260	0.268

Table 4. Atomic Orbital (AO) Population for the Pd of the Intermediates, Transition States, Products, and the Other Structures on the Reaction Coordinates of the Oxidative Addition of $C_4H_4XH_2$ (X = Sn, Ge, Si, C) to the ($H_2PC_2H_4PH_2$)Pd Complex 1 and the Intramolecular Rearrangement of 6sn

	4d						5p	
	xz	*yz*	*xy*	z^2	x^2-y^2	5s	*x*	*z*
5sn	1.922	1.947	1.769	1.951	1.874	0.366	0.002	0.000
TS2sn	1.902	1.953	1.925	1.952	1.894	0.328	0.002	0.001
a	1.876	1.958	1.872	1.946	1.903	0.374	0.002	0.001
b	1.924	1.963	1.765	1.951	1.923	0.405	0.002	0.001
6sn	1.944	1.956	1.651	1.965	1.923	0.500	0.003	0.001
TS3sn	1.840	1.937	1.929	1.943	1.906	0.363	0.002	0.002
TS4sn	1.939	1.906	1.689	1.948	1.936	0.380	0.002	0.002
TS2ge	1.942	1.952	1.813	1.948	1.932	0.356	0.002	0.001
TS2si	1.918	1.964	1.806	1.958	1.909	0.361	0.001	0.001
TS2c	1.931	1.962	1.707	1.954	1.915	0.374	0.001	0.002

the Pd−Sn distance is most shortened and increased again as the Sn−Pd−C^1 plane perpendicular to the P−Pd−P plane rotates to form **6sn**. The population of the Pd d_{z^2} orbital, which slightly contributes to the electron back-donation to the Sn, also gave a shallow minimum at point a. In contrast to this, the population of the Pd d_{xy} orbital indicated the opposite trend; it showed a maximum around the transition state **TS2sn** and decreased with the rotation of the Sn−Pd−C^1 plane. The population of both $d_{x^2-y^2}$ and s orbitals of the Pd which receive the electron donated from the Sn−C^1 σ orbital gradually increased during the reaction. These results suggest that the C−Sn bond is preliminary weakened in the *xz* plane by the electron back-donation from the Pd d_{xz} orbital in the first process of the reaction, and the bond breaking is finally completed in the *xy* plane by the electron back-donation from the Pd d_{xy} orbital enhanced by the electron donative phosphine ligands. The charge transfer interaction in the *xz* plane would significantly stabilize the transition state **TS2sn** and lower the energy barrier. We did not find the obvious change in the population of the Pd d_{xz} orbital during the reaction for X = Ge, Si, and C.

As mentioned earlier, the intermediate **5** is the hydrido complex in the case of X = Si. One of Si−H bonds is located in the vicinity of the Pd atom during the reaction due to the small van der Waals radius of the Si atom, so that the possibility of the contact of the σ and σ^* orbitals of the Si−H bond with the d and sp orbitals of the Pd remarkably increases. Although the angle δ of 52.5° in **TS2si** becomes 70.2° in structure **e** by the electronic repulsion between the occupied d_{xy} orbital and the C^1-H σ orbital (see above), the marked decrease in the population of the Pd d_{xz} orbital by the electron back-donation to the Si was not found. The Si−H σ orbital is strongly attracted by the Pd in structure **d** as shown by the Si−H bond stretched by 26% and the short Pd−H distance of 1.878 Å, because the electron donation from the polarized Si−H σ orbital to the Pd $d_{x^2-y^2}$+sp hybridized orbital is very facile. As

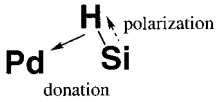

the dihedral angle δ enlarged to 95.9° decreases by further rotation of the Si−Pd−C^1 plane, the Si−H bond cleavage proceeds to form **5si** by electron back-donation from the Pd d_{xy} orbital to the Si−H σ^* orbital. However, in the case of X = C, not only C(X) but also C^1 are far away from the Pd in structure **f** without the approach of the C(X)−H bond to the Pd atom, because the polarization of both C(X)−H and C(X)−C^1 bonds are too small to promote electron donation and back-donation on the *xz* plane mentioned earlier. When the C^1−Pd−C^2 plane becomes nearly parallel to the P−Pd−P plane, the C^1═C^2 π orbital interacts with the Pd to form **5c** through electron donation and back-donation in the *xy* plane. In other words, after the breaking of the C^1═C^2 π interaction with the Pd and the subsequent rotation of the C(X)−Pd−C^1 plane into the *xy* plane are completed, the C(X)−C^1 bond is broken through the electron donation and back-donation in the *xy* plane. The slight twist of the C(X)−Pd−C^1 plane with $\delta = 17.1°$ in the transition state **TS2c** is ascribed to the electronic repulsion between the C−H σ orbitals and the occupied d_{xy} orbital of the Pd (see section 3.3).

The potential energy surfaces for X = Sn, Ge, Si, C are displayed together in Figure 5. The reaction starting from **5** is endothermic for all the cases. The potential energy surface is more stable than **1** except for the case of X = C and is most stabilized for X = Sn. As the stability of the transition state **TS2** increases (Sn > Si ≈ Ge > C), the energy barrier decreases (Si (11.5 kcal/mol) < Sn (15.3 kcal/mol) < Ge (20.7 kcal/mol) < C (47.9 kcal/mol)), except for the case of X = Si, in which the intermediate **5si** is the hydrido complex. The potential energy surface for X = C requires the largest energy barrier of 47.9 kcal/mol, because the d_{xz} orbital of the Pd atom does not incorporate at all in the transition state.

Also, it is of great interest that the transition state **TS3sn** between two **6sn** for the mutual switch of the positions of the Sn and C^1 atoms utilizing the apical site was found. The structural features of **TS3sn** are quite similar to those of **TS2sn**, and the Sn and C^1 atoms are located at the apical and equatorial positions, respectively, as presented in Figure 6. However, the Pd−Sn and Pd−C^1 distances are shorter while the Sn−C^1 and Pd−C^2 distances are longer compared with those of **TS2sn**, and the energy is only slightly lower than that of **TS2sn**. In **TS3sn**, the population of the d_{xz} orbital of the Pd atom largely decreases as well (see Table 4).

The potential energy surface of the C^2−C^2 bond breaking of stannole starting from the π-complex **5sn** is also presented in Figure 6, together with the optimized structures of the transition state **TS4sn** and the product **7sn**. The C^2−Pd−C^2 plane is exactly parallel to the P−Pd−P plane in the transition state **TS4sn** and never twists during the C^2−C^2 bond breaking. Therefore, the population of the Pd d_{xz} orbital does not change, whereas that of the Pd d_{xy} orbital largely decreases in **TS4sn** due to electron back-donation from the Pd d_{xy} to the C^2−C^2 σ^* orbital (see Table 4). The energy barrier of 53.2 kcal/mol is very large even with the contribution of the π orbitals on the C^2 atoms to the electron donation to the Pd in **TS4sn**.

3.3. Oxidative Addition of the C−X Bonds of CH_3XH_3 (X = Sn, Ge, Si, C) to the $(H_2PC_2H_4PH_2)$-Pd Complex. The optimized structures for the oxidative addition of the C−X bonds of CH_3XH_3 (X = Sn, Ge, Si, C) to the $(H_2PC_2H_4PH_2)$Pd complex are presented in Figure 7. As is well-known, the transition state of the H−H or C−H σ bond activation at the Pd of the phosphine-coordinated complex, $(PH_3)_2Pd$,[4,5] has a square planar structure, because the electron back-donation from the dπ orbital of the Pd enhanced on the P−Pd−P plane to the σ^* orbital as well as the donation from the σ orbital to the dσ+sp hybridized orbital of the Pd plays an important role in the bond breaking. However, the transition state **TS5** has a relatively large angle δ of 42−63° in each case of X = Sn, Ge, Si, C, similar structural features of the transition state having been theoretically obtained for the C−C and Si−C bond activation of CH_3CH_3 and SiH_3CH_3 on the $(PH_3)_2Pt$ complex by Sakaki et al.[19] The transition state structures for CH_3XH_3 are obviously different from those for heteroles (see section 3.2); the angle δ of 63.2° for X = Sn is much smaller, and in contrast, the angle δ of 42.9° for X = C is much larger, compared with the corresponding angle δ in the case of heteroles. It would be most plausible to think that the steric repulsion not between the CH_3XH_3 and the phosphine ligand moieties but between the C−H σ orbital of CH_3XH_3 and the occupied Pd d_{xy} orbital causes the twist of the X−Pd−C plane in the transition state, since the $(H_2PC_2H_4PH_2)$-Pd complex used in the present study provides enough reaction space even in the initial stage of the reaction due to the chelate phosphine ligand with the small bite angle. In fact, the Pd−H(−C) distance of 2.2−2.3 Å is short in the transition state for all the cases.

No explicit change in the population of the Pd d_{xz} orbital was found in the transition state for all the cases, which indicates that the Pd d_{xz} orbital does not participate in the activation reaction. Even for X = Sn, electron back-donation from the Pd d_{xz} orbital to the Sn in the *xz* plane mentioned in section 3.2 does not occur, although the C−Sn bond of CH_3SnH_3 is strongly polarized as well as that of stannole (see Table 3). The crucial difference between stannole and CH_3XH_3 can be found on the carbon; the carbon of CH_3XH_3 lacks the π orbital. The lobe of the π orbital directed to the Pd atom would efficiently support the electron donation to the Pd atom. Thereby, the electron deficiency at the Sn atom is further strengthened and then electron donation from the Pd d_{xz} orbital to the Sn is greatly induced. This disadvantage of CH_3SnH_3 is reflected in the energy barrier of 21.5 kcal/mol, which is larger by 6.2 kcal/mol than that for stannole (see Figures 5 and 8).

On the other hand, the polarized X−H bond in the vicinity of the Pd atom in the transition state **TS5** is readily broken without energy barrier to form the hydrido complex **8** except for the case of X = C, which is similar to the case of heterole with X = Si (section 3.2), because the electron donation from the polarized X−H (X = Sn, Ge, Si) σ orbital to the Pd is facile. Here,

(19) Sakaki, S.; Mizoe, N.; Musashi, Y.; Biswas, B.; Sugimoto, M. *J. Phys. Chem. A* **1998**, *102*, 8027.

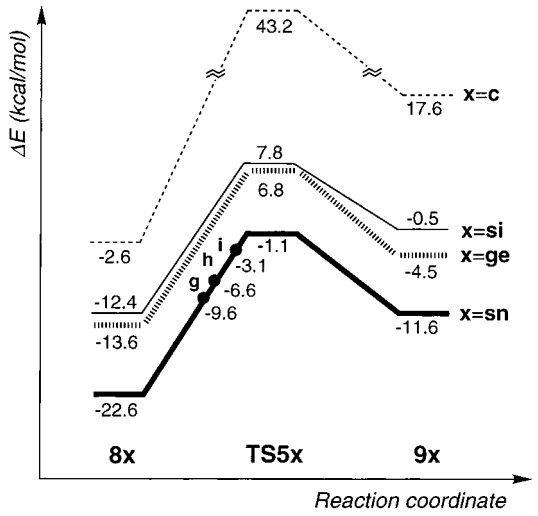

Figure 8. B3LYP/BSI potential energy surfaces (in kcal/mol) of the oxidative addition of the C−X bonds of CH_3XH_3 (X = Sn, Ge, Si, C) to the $(H_2PC_2H_4PH_2)Pd$ complex **1**. The boldface, boldface-dotted, normal, and dotted lines are for X = Sn, Ge, Si, C, respectively. The energies relative to **1** are presented.

it should be noted again that the X−H bond approaches the Pd atom perpendicularly to the P−Pd−P plane, avoiding the steric contact between the occupied d_{xy} orbital and the C−H σ orbital. This is revealed by the serial snapshots of the structure on the potential energy surface from point i to g, **i**→**h**→**g**, for X = Sn. However, the X−H bond cleavage is finally completed on the *xy* plane by electron back-donation from the Pd d_{xy} orbital to the X−H σ* orbital. In the case of X = C, the C(X)−H bond, which is not polarized, is not broken but attracted by the Pd atom, as shown by **8c**.

The potential energy surfaces for X = Sn, Ge, Si, and C are presented together in Figure 8. Their shapes are the same, and the reaction is endothermic for all the cases. The potential energy surfaces are stabilized in the order Sn > Ge> Si > C, according to the sequence in the interaction of the atom X with the Pd, Sn > Ge > Si > C. There was no explicit tendency in the energy barrier, which is about 20−22 kcal/mol for X = Sn, Ge, Si, aside from the case for X = C, with the large energy barrier of 45.8 kcal/mol.

3.4. Possibility of Intramolecular Rearrangement of the $(H_2PC_2H_4PH_2)Pd(H)(XH_3)$ (X = Sn, Ge, Si, C) Complexes. Since the reaction path for the intramolecular rearrangement of **6sn** which mutually switches the positions of the C and Sn atoms via the transition state **TS3sn** was found as mentioned in the section 3.2, we examined the possibility of such rearrangement on the hydrido complexes $(H_2PC_2H_4PH_2)Pd(H)(XH_3)$ (X = Sn, Ge, Si, C). To exchange the positions between the hydrido and XH_3 ligands on the $(H_2PC_2H_4PH_2)Pd(H)(XH_3)$ complex without the dissociation of XH_4, the X−H axis has to become perpendicular to the P−Pd−P plane in the transition state. However, the perpendicular approach of the X−H bond to the Pd would be extremely unfavorable in energy, as it is well-known that the transition state of the activation of the X−H bonds of XH_4 on the $(PH_3)_2M$ or $(H_2PC_2H_4PH_2)M$ (M = Pd, Pt) complexes has a square planar structure.[3b,4,5,19,20] In fact, the transition state for such intramolecular rearrangement did not exist for the $(H_2PC_2H_4PH_2)Pd(H)(CH_3)$ complex, due to the dissociation of the CH_4 molecule. However, it was revealed that the intramolecular hydrido-SnH_3 ligand exchange on the $(H_2PC_2H_4PH_2)Pd(H)(SnH_3)$ complex is possible in principle, although the energy barrier is very large, as presented in Figure 9. The Sn−Pd−H plane is exactly perpendicular to the P−Pd−P plane, and the hydrido and the SnH_3 occupy the equatorial and the apical positions, respectively, in the transition state **TS6sn**. Although the Sn−H distance is shortened to 1.886 Å, the Pd−Sn and Pd−H distances are only 3−4% stretched, indicating that both Pd−Sn and Pd−H interactions remain strong in **TS6sn**. The contribution of the apical site in **TS6sn** is obvious. As shown in Table 5, the population of the Pd d_{xz} orbital is reduced to 1.841*e*, while that of the Pd s orbital increased to 0.355*e* in **TS6sn**. This is reasonably understood on the basis of the fact that the Sn−H bond is strongly polarized (see Table 3). That is, the largely negatively charged hydrido at the equatorial position donates the electron to the Pd s orbital, and the electron-deficient Sn receives the electron from the Pd d_{xz} orbital. It is worth noting that the SnH_4 hydrogen without the π orbital as well as the stannole C^1 with the π orbital functions at the equatorial position. The small size of the SnH_4 hydrogen can come closely to the Pd to donate the electron, avoiding electronic repulsion. Nevertheless, the transition state **TS6sn** is unstable in energy due to the lack of π orbital, which efficiently supports the electron donation.

When the Sn atom is replaced by the Ge or Si atom, the features of the transition state are changed. The angle ∠m−Pd−X becomes larger and the obvious distinction in the position between the XH_3 and hydrido ligands disappears, although the X−Pd−H plane remains perpendicular to the P−Pd−P plane. The X−H distance is shortened, while the Pd−H distance is lengthened. These results indicate that both the electron donation from the hydrido to the Pd and the back-donation from the Pd d_{xz} orbital to the atom X are weakened. Indeed, the population of the Pd d_{xz} orbital is much larger and that of the Pd s orbital is much smaller for Ge and Si than for Sn, as presented in Table 5. This is ascribed to the polarization of the X−H bond, which is weaker for Ge and Si than for Sn (see Table 3). The transition state is less stable in energy for Ge and Si than for Sn, consistently.

Surprisingly, another Sn−H bond of **10sn** is further activated in the plane perpendicular to the P−Pd−P plane. The reaction proceeds with an energy barrier of 26.4 kcal/mol passing through the transition state **TS7sn** to form the dihydrido-stannylene complex **11sn**. Two hydrido ligands and the SnH_2 are at the equatorial and apical positions, respectively, in **11sn**. The unoccupied p orbital of SnH_2 interacts with not only the Pd atom but also one of the electron-rich hydrido ligands. Therefore, the SnH_2 coordinated to the Pd with the Pd−Sn distance of 2.803 Å inclines toward one

(20) It was found that the activation of the X−H (X = Sn, Ge, Si) bonds of XH_4 at the Pd of $(H_2PC_2H_4PH_2)Pd$ takes place in the P−Pd−P plane without an energy barrier.

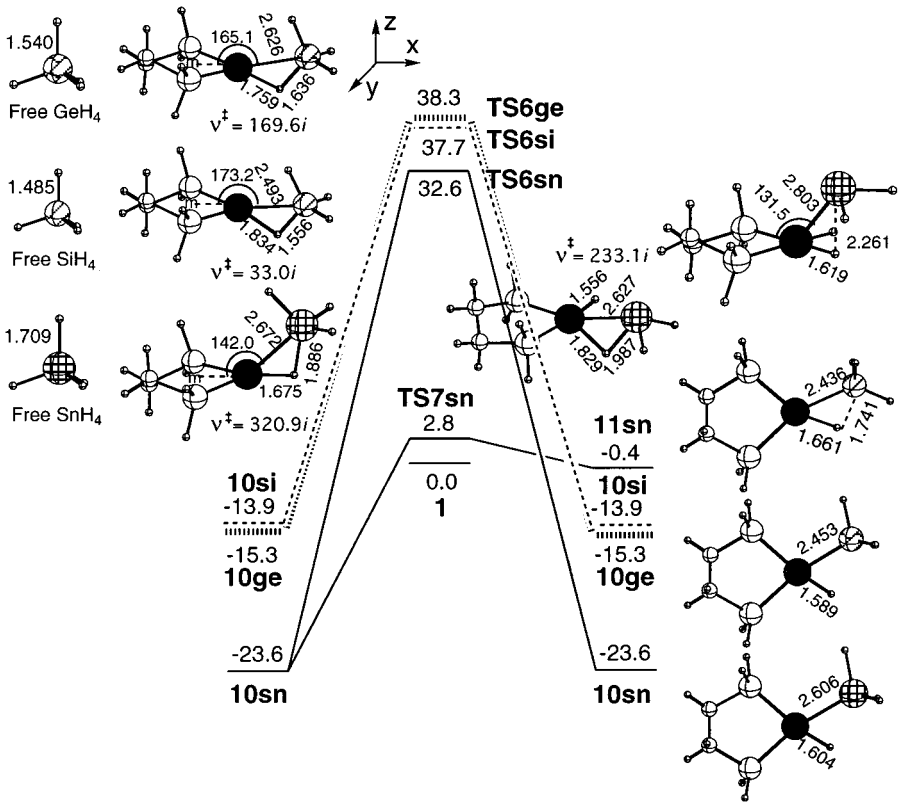

Figure 9. B3LYP/BSI potential energy surfaces (in kcal/mol) of the intramolecular rearrangement of the hydrido complexes $(H_2PC_2H_4PH_2)Pd(H)(XH_3)$ (X = Sn, Ge, Si) **10** through the transition states **TS6** (**10**→**TS6**→**10**), and the Sn−H bond activation of the hydrido complex **10sn** (**10sn**→**TS7sn**→**11sn**), together with the optimized structures (in Å and deg) of the transition states **TS6** and **TS7**, the hydrido complexes **10** and **11**, and the free XH_4 at the B3LYP/BSI level. The imaginary frequencies (cm^{-1}) are shown for the transition states **TS6** and **TS7sn**. m is the midpoint between two P atoms. The energies relative to **1** are presented.

Table 5. Atomic Orbital (AO) Population for the Pd of the Transition States TS6 on the Intramolecular Rearrangement of the Hydrido Complexes $(H_2PC_2H_4PH_2)Pd(H)(XH_3)$ (X = Sn, Ge, Si) 10 and the $(H_2PC_2H_4PH_2)Pd$ Complex 1

	4d						5p	
	xz	*yz*	*xy*	z^2	x^2-y^2	5s	*x*	*z*
1	1.933	1.946	1.916	1.956	1.922	0.294	0.001	0.001
TS6sn	1.841	1.976	1.941	1.967	1.928	0.355	0.002	0.000
TS6ge	1.904	1.973	1.928	1.956	1.925	0.309	0.002	0.000
TS6si	1.922	1.974	1.916	1.947	1.929	0.281	0.002	0.000

of the hydrido ligands with the large ∠P−Pd−Sn angle of 131.5°. A similar reaction path did not exist for X = Ge, Si.

4. Concluding Remarks

We have successfully indicated the importance of the apical site of the $(H_2PC_2H_4PH_2)Pd$ complex on some elementary reactions using the density functional method (B3LYP). On the phosphine-coordinated palladium complex, the role of the fifth site at the apical position has not been known so far according to our knowledge, because, for example, the elementary reactions such as oxidative addition and reductive elimination of the chemical bonds usually take place in the equatorial plane by charge transfers between the d and sp orbitals of the Pd enhanced by the equatorial phosphine ligands and the bonding and antibonding orbitals of the chemical bonds. However, in the present study, it was found that the apical site of the palladium complex plays an important role in some cases; the charge transfer from the Pd d orbital to the substrate at the apical site significantly stabilizes the potential surface of the reaction and lowers the energy barrier.

In the insertion of XH_2 (X = Sn, Ge, Si, C) into the Pd−C bond of the $(H_2PC_2H_4PH_2)Pd(\eta^2\text{-HC}\equiv\text{CH})$ complex, the free XH_2 first coordinates to the apical site of $(H_2PC_2H_4PH_2)Pd(\eta^2\text{-HC}\equiv\text{CH})$ through the charge transfer, and the effect of the apical site to promote the reaction increases in the order Sn < Ge < Si. On the other hand, in the oxidative addition of the C−X bonds of heteroles, this order is reversed, i.e., Sn > Ge > Si > C, because the charge transfer from the Pd d orbital to the atom X at the apical site increases in the order Sn > Ge > Si > C, depending on the polarization of the C−X bonds. However, the apical site is invalid for the oxidative addition of the C−X bond of CH_3XH_3 without the π orbital on the carbon, which promotes the charge transfer at the apical site. We also theoretically suggested that an intramolecular rearrangement of the $(H_2PC_2H_4PH_2)Pd(H)(SnH_3)$ complex which mutually switches the positions of the hydrido and SnH_3 ligands is possible with the support of the apical site. Surprisingly, another Sn−H bond was further activated in the plane perpendicular to the P−Pd−P plane on the $(H_2PC_2H_4PH_2)Pd(H)(SnH_3)$ complex, which produces $(H_2PC_2H_4PH_2)Pd(H)_2(SnH_2)$ with stannylene at the apical position. The importance of the apical site in these reactions strongly depends on the atom X.

Acknowledgment. The calculations were in part carried out at the Computer Center of the Institute for Molecular Science, Japan. T.M. was partly supported by Grants-in-Aid from the Ministry of Education, Science, Sports, and Culture, Japan.

Supporting Information Available: Listings giving the optimized Cartesian coordinates of all equilibrium structures and transition states presented in this paper. This material is available free of charge via the Internet at http://pubs.acs.org.

OM020119B